Fall 8-6-2012

Long reach cantilevers for sub-cellular force measurements

Govind Paneru

Prem S. Thapa

Sean P. McBride
Marshall University, mcbrides@marshall.edu

Recommended Citation

Paneru, G., Thapa, P. S., McBride, S. P., Ramm, A., Law, B. M., & Flanders, B. N. (2012). Long reach cantilevers for sub-cellular force measurements. Nanotechnology, 23(45), 455105.

Long reach cantilevers for sub-cellular force measurements

Govind Paneru,[1] Prem S. Thapa,[2] Sean P. McBride,[1] Adam Ramm,[1] Bruce M. Law,[1] and Bret N. Flanders[1,a)]
[1]Department of Physics, Kansas State University, Manhattan, KS 66506-2601
[2]Imaging and Analytical Microscopy Lab, University of Kansas, Lawrence, Kansas 66045, USA

[a)]Electronic mail: bret.flanders@phys.ksu.edu

SUBMITTED 06/09/2012, REVISED 8/06/2012

Abstract. *Maneuverable*, high aspect ratio poly 3-4 ethylene dioxythiophene (PEDOT) fibers are fabricated for use as cellular force probes that can interface with individual pseudopod adhesive contact sites without forming unintentional secondary contacts to the cell. The straight fibers have lengths between 5 and 40 μm and spring constants in the 0.07-23.2 nN μm^{-1} range. The spring constants of these fibers were measured directly using an atomic force microscope (AFM). These AFM measurements corroborate determinations based on the transverse vibrational resonance frequencies of the fibers, which is a more convenient method. These fibers are employed to characterize the time dependent forces exerted at adhesive contacts between apical pseudopods of highly migratory *D. discoideum* cells and the PEDOT fibers, finding an average terminal force of 3.1 ± 2.7 nN and lifetime of 23.4 ± 18.5 s to be associated with these contacts.

1. Introduction

Pseudopod-facilitated motility is a critical aspect of the amoeboid migration exhibited by *D. discoideum*, neutrophils, T lymphocytes [1], and other highly migratory cells [2]. These cells crawl at rates as large as ~30 μm min^{-1} to forage for micro-organisms and antigens in their local environments [3]. To achieve such high speeds, the cells must adhere to and release the supporting substrates quickly. Pre-aggregative (*i.e.* migratory) *D. discoideum*, for example, were recently reported to form adhesive contacts (called actin foci) that form and decay on ~20 s time scales [4]. The short-lived nature of these contacts differs significantly from the ~20 min lifetimes of the *focal adhesion complexes* used by slow-migrating cells like keratinocytes and fibroblasts [5]. In contrast to focal adhesion complexes, which have been intensively studied at the single complex level for over a decade [6-8], comparatively little is known about the adhesive structures and dynamics of highly migratory cells.

The amoeboid paradigm of cellular movement [9, 10] essentially consists of reception of stimuli

(*e.g.* a signaling molecule at a cell-surface receptor) followed by the localized protrusion of exploratory appendages, such as pseudopods, from the cell. A typical pseudopod [figure 1(a)] is a few microns in length and has a submicron tip size. A cell may protrude many pseudopods at a given time. Commonly, the pseudopod will adhere its foremost tip to the local substrate [9-11]. Contraction of the actin cytoskeleton along the pseudopod-axis (by molecular motors) pulls the cell towards the adhesive contact. The molecular-level mechanisms by which pseudopods adhere to substrates for both *D. discoideum* and *amoeboid* leukocytes are not known [12, 13]. However, these are the first contacts that the cell makes with the anterior substrate, and the traction forces exerted against the substrate at these sites dictate the cell's instantaneous direction-of-migration. Hence, they are a key aspect of amoeboid motility. Characterization of the dynamical forces exerted at these contacts would constitute a key step towards resolving the potential energy surface associated with the adhesion and, ultimately, controlling the transient adhesive contact mechanism in highly migratory cells.

A variety of methods are used to characterize the forces that cells exert at their adhesive substrate-contacts. The deformable substrate technique measures cell-induced wrinkling or marker-displacement within an elastic substrate [14]. This approach does not directly measure the forces exerted at the individual contacts, but rather extracts them by modeling the deformation-map induced by the whole-cell. This can be a non-trivial undertaking [15]. Approaches that utilize atomic force microscopy (AFM) provide excellent resolution of the dynamical forces exerted between cells and substrates [16]. *Single-cell force spectroscopy* [17] entails the attachment of a living cell to an AFM cantilever that is then lowered into contact with a substrate. The substrate is typically functionalized with a ligand of interest (*e.g.* fibronectin) [18, 19]. The force on the AFM cantilever is then measured as the cantilever-cell unit is retracted from the substrate. This method has shed light on a wide range of ligand-receptor adhesive interactions [20-22], as have the conceptually similar biomembrane force probe [23] and laser trap [24] methods. A challenge for such cell-as-probe techniques lies in minimizing the contact area to a single, cell-initiated adhesive contact: that between a pseudopod tip and a substrate, for example.

What is needed is a long, thin probe that can interface with targeted sites, such as the adhesive contacts of pseudopods, without forming unintentional secondary contacts to the cell. Therefore, this study presents a methodology for fabricating and calibrating high aspect ratio PEDOT fibers for use as cellular force probes. These cantilevers are an improvement over on-chip PEDOT force sensors reported recently [25] because these cantilevers are considerably easier to calibrate, and they may be maneuvered independently around a cell and, permitting both lateral and apical (topside) targets on the cellular surface to be probed. This capability enables interrogation of the off-plane, pseudopod-facilitated motility that occurs in nature when amoeboid cells migrate through 3D matrices.

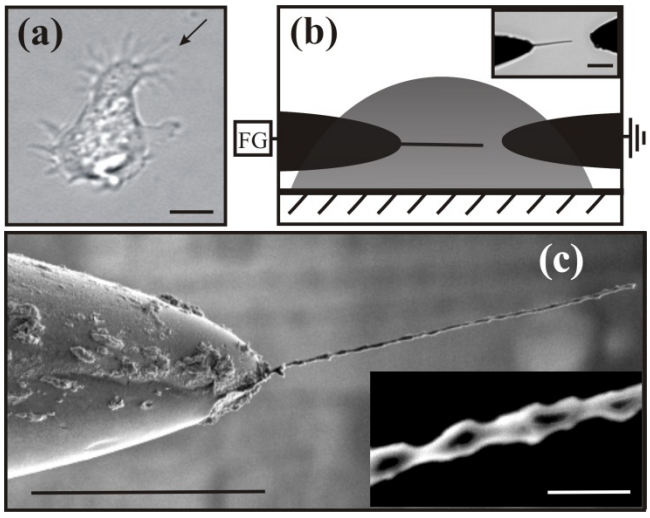

Figure 1. (a) Optical micrograph of a *D. Discoideum* cell extending pseudopods. A pseudopod is indicated by the arrow. Scale bar = 5 μm. (b) Schematic depicting the side-view of the experimental set-up for PEDOT fiber growth. FG designates a function generator. Inset: optical micrograph depicting the bottom view of the set-up. Scale bar = 10 μm. (c) SEM image of a PEDOT fiber grown from an etched tungsten tip. Scale bar = 20 μm. Inset: enlarged view of the fiber. Scale bar 1μm.

2. Experimental Methods

Direct characterization of a ~400 nm wide pseudopod [see figure 1(a)] requires a probe of comparable dimension. The probe should also have a sufficiently high aspect ratio to allow it to cleanly reach a targeted site without forming unintentional, secondary contacts with the cell. To meet these requirements, we have fabricated cantilevered force sensors composed of poly(3,4-ethylene dioxythiophene) (PEDOT)

fibers grown from the tips of etched tungsten wire. The bottom 5 mm of a vertically oriented, electrically grounded tungsten filament (0.019 in diameter, SmallParts) were electro-etched by repeated dipping over a ~4 min period into a 10 M $NaNO_2$ 6MKOH solution that was biased at +4 V, as described elsewhere [26]. This procedure yields conical tips with radii-of-curvature of ~1 μm or less. Reproducibility was optimized by using a sewing machine to cycle the filament in and out of solution at a rate of ~10 s^{-1}. We used the simple polymerization technique *directed electrochemical nanowire assembly* (DENA) to grow the PEDOT fiber from the tip of the tungsten filament [27-29]. Briefly, the tungsten filament was first evaporatively coated with ~200 nm of Au to promote strong attachment of the polymer. After mounting the coated filament in a 3D stage and positioning it ~1 μm above a microscope slide, a 20 μL aliquot of aqueous solution containing 0.01 M 3,4-ethylene dioxythiophene and 0.02 M poly(sodium styrene sulfonate) was deposited across the ~30 μm gap between the wire tip and an Au counter-electrode that was similarly mounted. Figure 1(b) is a schematic of this arrangement. A square wave voltage signal (±3.5 V, 10.0 kHz) was applied to the electrodes to induce PEDOT nano-fiber growth via electrochemical polymerization [30]. As explained elsewhere, the voltage-frequency sets the average radii of the fibers during growth [30], but spatio-temporal fluctuations in the polymerization rate of the amorphous PEDOT material give rise to radial variation (~50%) about the mean radius [28, 29]. The voltage signal is terminated after a few seconds when the PEDOT nano-fiber reaches the desired length. Translation of the microscope stage pulls the solution-drop away from the nano-fiber, straightening it due to the tension at the air-filament-solution contact line. The nano-fibers retain their straightened geometries upon re-immersion in aqueous solution. A scanning electron micrograph of a typical straightened nano-fiber is shown in figure 1(c).

We have used an atomic force microscope (AFM, *Model:* MFP-3D, Asylum Research) to directly measure the spring constants k_F of the PEDOT fibers, as detailed elsewhere [25]. Briefly, this was done by lowering a calibrated AFM cantilever (CSC12/tipless, MikroMasch) of spring constant k_C against an

individual fiber in order to deflect it by distance Δz, as illustrated in figure 2(a) and plotted in figure 2(b) [31]. When the opposing forces exerted by the fiber and the cantilever are equal in magnitude, the following expression relates the spring constant of the fiber to the measured quantities [32, 25]:

$$k_F = k_C\left(\Delta z / \delta_C - 1\right)^{-1}\left(\frac{L-\Delta L}{L}\right)^3 \cos^{-2}\theta. \qquad (1)$$

δ_c is the deflection of the cantilever and L is the length of the fiber. The tilt angle θ of the AFM cantilever was 11° for all cases in this study. The position of contact from the end of the fiber ΔL was measured via an internal optical microscope in the AFM.

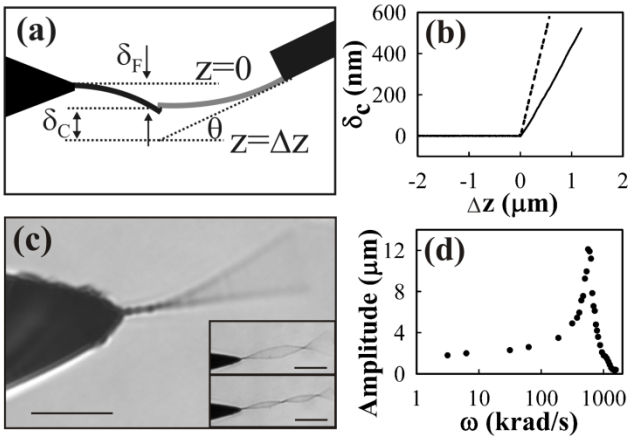

Figure 2. (a) Schematic of AFM-based set-up for measuring the spring constant of a PEDOT fiber. (b) AFM cantilever deflection magnitude δ_C versus vertical position of AFM head Δz for pressure against a rigid surface (dashed profile) and a PEDOT fiber (solid profile). (c) Optical micrograph of a PEDOT fiber resonating at its fundamental frequency. Scale bar = 15 μm. Inset: optical images of a PEDOT fiber resonating in its first (upper) and second (lower) harmonic modes. Scale bar = 15 μm. (d) Amplitude versus driving frequency plot for the PEDOT fiber in panel (c).

We have also determined the spring constants of the PEDOT cantilevers by the resonance-frequency method, which is technically simpler than the AFM method [33]. To measure the resonance frequency of a PEDOT fiber, we position this single PEDOT cantilever ~10 μm from an Au counter-electrode. A ± 20 V square wave voltage-signal of frequency f and a +20 V DC offset are applied to the PEDOT cantilever while the Au electrode is grounded [34]; polarization forces drive transverse oscillation of the PEDOT fiber at this frequency. A bright field image of a cantilever resonating in its fundamental mode is shown in figure 2(c). Images of the vibrating fiber are collected as f is increased in

5 kHz steps. A representative amplitude vs angular frequency plot is depicted in figure 2(d), where the angular frequency ω is defined as $\omega = 2\pi f$. The frequency at which the amplitude reaches its first maximum locates the fundamental resonance frequency ω_0 [565 krad s^{-1} in figure 2(d)]. Amplitude maxima at frequencies of half the observed resonance frequency were not observed, and the vibrational amplitude was directly proportional to the voltage-amplitude, confirming that the reported ω_0-values are fundamental frequencies [33]. The resonances of the tungsten filament are well-below those of the PEDOT cantilever and, hence, do not complicate these measurements. The spring constant k_{res} of a radially uniform and solid cantilevered rod of length L depends on ω_0 as

$$k_{res} = 0.08\frac{\pi\rho_m{}^2 L^5}{E}\omega_0{}^4. \qquad (2)$$

ρ_m is the mass density of the fiber material (PEDOT) and E its Young's modulus. (2) was derived by using the expression for ω_0 of a radially uniform rod $\omega_0 = 1.75\sqrt{E\rho^{-1}}rL^{-2}$ to eliminate r in the expression for the spring constant k of a uniform rod $k = \frac{3\pi E r^4}{4L^3}$ [35]. As explained below, (2) was used to predict the spring constants of the PEDOT fibers.

Type KAx3 *D. discoideum* cells [36], grown at 24 ^{o}C, were removed from HL-5 culturing medium by drawing 1000 μL of the cell-medium suspension from a Petri dish and centrifuging the aliquot for ~10 s at 1.34×10^3 g. The supernatant was discarded and the cells were washed two times with 12 mM phosphate buffer and shaken before suspending the cells a final time in phosphate buffer and starving them for 4-6 hours. 50 μL volumes of cell suspension and phosphate buffer were deposited in the side-view imaging chamber described below. A waiting time of ~20 minutes, following cell deposition, was required for the cells to settle and begin migrating on the surfaces of the chamber.

To facilitate investigation of apical pseudopods, which are important for amoeboid migration through 3D matrices, cells were visualized *in profile* so that the size, shape and cellular location of the

pseudopod-fiber contact could be clearly observed. This mode requires that the imaging plane of the microscope be perpendicular to the substrate on which the cell crawls. Our set-up for realizing this perspective, which differs from that reported elsewhere [37], is diagrammed in figure 3(a). Briefly, a hole was bored in the base of a Petri dish (Fisherbrand) using a 7/32" drill bit at 990 rpm; these parameters minimized lip and sidewall roughness (~3 μm). A cover-slip was cemented to the underside of the dish to seal the hole. *D. discoideum* cells were cultured and introduced to the chamber at cell surface densities of ~10^3 mm^{-2}. The dish was mounted on the stage of an inverted microscope (Leica IRB) for optical imaging, primarily with a 63× water immersion objective of 0.90 numerical aperture. Side-view imaging of the cells was accomplished by focusing the microscope on those migrating on the sidewalls of the hole. A typical side-view image of a *D. discoideum* cell is shown in figure 3(b). The arrow points to an apical pseudopod.

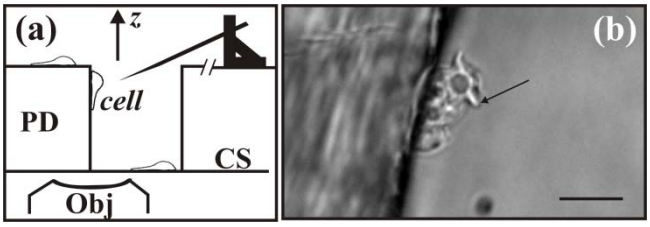

Figure 3. (a) Schematic (not to scale) of the side-view imaging set-up depicting the Petri dish (PD), cover-slip (CS), and microscope objective (Obj). (b) Side-view micrograph of a *D. Discoideum* cell extending apical pseudopods. The apical pseudopod indicated by the arrow is 2.5 μm long and ~400 nm wide. Scale bar = 10 μm.

3. Results

We have directly measured the spring constants of 15 different PEDOT fibers by using an AFM as described above. The measured k_C, $\delta_C/\Delta z$, L, and ΔL values were substituted into (1) to obtain the corresponding k_F determinations. Each fiber was characterized 3 times. The average of the three k_F determinations is denoted $\bar{k}_F$. All quantities required to make these spring constant determinations are reported in Table 1 (fibers 1-15).

Table 1: Parameters for the Spring Constant Measurements.

Fiber	L (μm)	$\frac{\delta_C}{\Delta z}$	ΔL (μm)	k_C (nN/μm)	k_F (nN/μm)	$\overline{k_F}$ (nN/μm)	ω_0 (krad/s)	r_{res} (nm)	k_{res} (nN/μm)
1	7.22	0.28	0.5	58	18.9	18.0	7850	202	21.0
2	14.58	0.34	6.56	58	5.3	5.1	2292.2	241	5.1
3	15.08	0.22	6.56	61	3.2	3.1	2009.6	226	3.6
4	9.66	0.41	2.2	61	20.2	19.0	5149.6	238	16.7
5	10.66	0.45	3.9	64	13.6	13.8	4207.6	237	12.2
6	8.80	0.41	3.06	60	12.1	12.1	5338	204	12.1
7	8.74	0.47	2.18	60	23.2	23.2	6091.6	230	19.8
8	12.39	0.3	4.8	61	6.2	6.1	2888.8	219	5.7
9	7.94	0.55	3	65.9	20.1	21.6	6908	216	20.3
10	10.36	0.5	3.06	60.8	22.1	21.4	5024	267	21.5
11	9.19	0.34	2.18	60.8	14.3	14.0	5149.6	215	13.0
12	9.72	0.54	3.93	65.3	16.7	16.7	4961.2	232	14.8
13	9.36	0.49	3.5	65.3	15.6	16.3	5275.2	229	15.7
14	10.83	0.37	4.37	62.8	8	8.2	3705.2	215	7.9
15	8.44	0.36	2.6	61	11.7	11.0	5212.4	184	8.9
16	12.84	-	-	-	-	-	2449.2	200	3.6
17	17.0	-	-	-	-	-	1382	198	1.5
18	20.0	-	-	-	-	-	1118	221	1.4
19	23.0	-	-	-	-	-	942	247	1.4
20	24.0	-	-	-	-	-	816	232	1.0
21	28.41	-	-	-	-	-	439.6	176	0.2
22	34.0	-	-	-	-	-	377	216	0.3
23	30.0	-	-	-	-	-	565	252	0.7
24	41.0	-	-	-	-	-	220	183	0.07
25	16.73	-	-	-	-	-	1758.4	244	3.5

Figure 2(c) shows a PEDOT fiber (23 in Table 1) resonating in its fundamental mode at 90 kHz. (It also resonates in its harmonic modes, as the insets show, demonstrating its strong elastic character). Figure 2(d) is the amplitude versus frequency plot for the fiber of panel (c), indicating a fundamental resonance frequency ω_0 of 565×10^3 rad s^{-1}. By substituting this ω_0 value into (2), we obtain a prediction of its spring constant k_{res} of 7.0×10^{-4} N m^{-1}. In calculating this result, we took the PEDOT Young's modulus E to be 2.0 GPa, the average of two recent determinations (1.8 GPa [38] and 2.26 GPa [39]), and the mass density ρ_m to be 1500 kg m^{-3} [40]. By using (2) we implicitly assume that a radially non-uniform

PEDOT fiber of length *L both* resonates *and* bends like a hypothetical PEDOT fiber of a constant radius (and length *L*). This relation is not generally true of structurally non-uniform fibers. Therefore, in figure 4(a) we have assessed the extent to which the resonance-based determinations are accurate by plotting the measured k_{res} values for 15 fibers against their measured $\bar{k}_F$ values. All parameters required to attain these k_{res} values are listed in Table 1 (Fibers 1-15). These data are best-fit by a line having a near unity slope of 0.95. It is clear that the k_{res}-values predict the spring constants of the PEDOT cantilevers with reasonable accuracy; moreover, in the small *k* range (~4 nN μm^{-1}) used in the cellular force application,

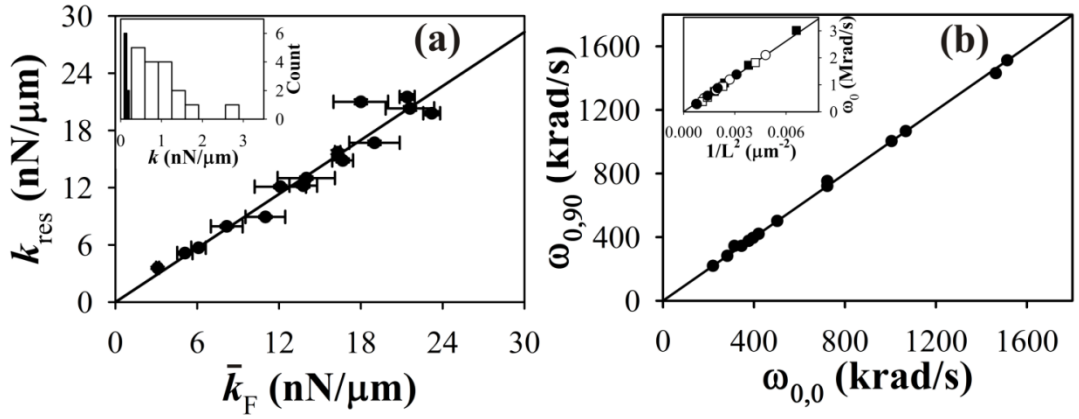

Figure 4. (a) Plot of resonance-based spring constant determinations k_{res} versus those measured by AFM $\overline{k_F}$ (filled circles). The solid line (constrained to pass through the origin) is the best fit to the points. The horizontal error bars denote the standard deviation of the mean associated with the $\bar{k}_F$ determinations; the vertical error bars, which are nearly too small to see, denote the propagated uncertainty in measuring ω and *L*. *Inset*: Distributions of the spring constants of fibers grown at 10.0 kHz to a length of 23.8 ± 0.8 μm (unfilled vertical bars) and at 20.0 kHz to a length of 23.4 ± 1.9 μm (filled vertical bars). (b) Plot of the fundamental resonance frequencies of PEDOT fibers $\omega_{0,0}$ against those measured when the fibers were axially rotated by 90° $\omega_{0,90}$. The solid line through the data points (filled circles) has a slope of unity. *Inset*: Plot of ω_0 for single fibers that were shortened (by breaking their tips) three times versus the inverse square of their lengths $1/L^2$. The solid line is a best fit through the data points. The four data-sets (circles, squares, unfilled circles, and unfilled squares) correspond to four different fibers.

the agreement is excellent. Hence, the resonance frequency calibration method, though approximate, is sufficiently accurate to justify forgoing the somewhat laborious AFM method. Fibers 16-24 in Table 1, several of which were too compliant for the AFM method, were characterized using the resonance frequency method.

The inset to figure 4(a) depicts two spring constant distributions corresponding to two sets of fibers grown with different frequencies of the alternating voltage to approximately the same lengths. As described elsewhere [30], the frequency of the alternating voltage sets the average radii of the fibers, with higher frequencies producing thinner fibers. One distribution (unfilled vertical bars) describes 14 fibers grown using a frequency of 10.0 kHz to a length of 23.8 ± 0.8 μm (unfilled vertical bars). The average spring constant for these fibers is 0.8 ± 0.6 nN/μm. The other distribution (filled vertical bars) describes 8 fibers grown using a frequency of 20.0 kHz to a length of 23.4 ± 1.9 μm. The average spring constant of these fibers is 0.08 ± 0.04 nN/μm. Hence, the spring constants of the fibers may be controlled across reasonably narrow ranges by controlling the frequency of the alternating voltage during growth, as well as the length of the fiber.

To assess the degree to which the structural non-uniformity of the fibers causes anisotropy in their spring constants, we have measured the ω_0-values in planes-of-bending that differ by 90^o of axial rotation. These resonance frequency values are denoted $\omega_{0,0}$ and $\omega_{0,90}$. Figure 4(b) plots the measured $\omega_{0,90}$-value against the corresponding $\omega_{0,0}$-value for 12 different fibers. These data are well-fit by a line of unity slope, indicating that the $\omega_{0,0}$ and $\omega_{0,90}$ values for a given fiber are equal. Another concern is that the fibers grow unevenly such that their tips have different average thicknesses than their bases. The inset to figure 4(b) plots ω_0 for single fibers that were shortened (by breaking off their tips) three times versus the inverse square of their lengths $1/L^2$. The different symbols represent the data-sets for the four fibers that were examined in this manner. These data lie along a single line, as indicated by the best-fit (solid line).

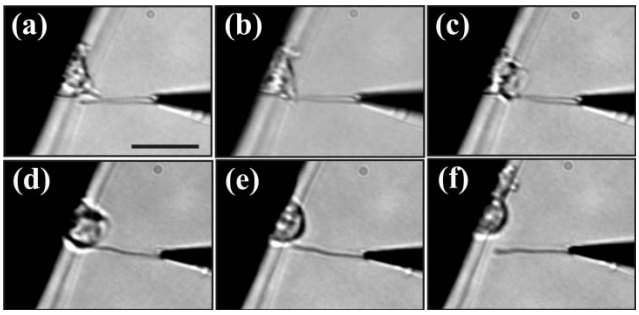

Figure 5. A series of optical micrographs of cantilevered PEDOT fiber (a) in its neutral position after contact initiation by the pseudopod; (b)-(d) while being deflected upwards by the cell at times 22 s, 68 s, 98 s, and 100 s respectively; and (f) at time 118 s when the fiber is back in its neutral position after release by the cell. A video of this event shown at ~6 × the actual rate is available online (AVI type, file size 677 KB, stacks.iop.org/Nano/2X/XXXXXX). The scale bar in panel (a) denotes 15 μm.

Figures 5(a)-(f) constitute a series of side-view images of a *D. discoideum* cell migrating on the vertical side-wall. An apical pseudopod adheres to the cantilever in panel (a), deflects it by exerting a pulling force on it in panels (b)-(d), and releases it in panel (e). A video of this event, shown at ~6 × the actual rate is available as supporting information (available at stacks.iop.org/Nano/2X/XXXXXX). These images depict an apical pseudopod-cantilever deflection event, where the cantilever represents a secondary substrate. The measured deflection $\delta_F(L)$ of the fiber is extracted from these images by finding the distance between the tip of the deflected and undeflected fiber. (Drift of the microscope stage occurred at a rate of 0.09 μm/min and, therefore, does not compromise the $\delta_F(L)$ determinations). The shape of the pseudopod evolves throughout this event.

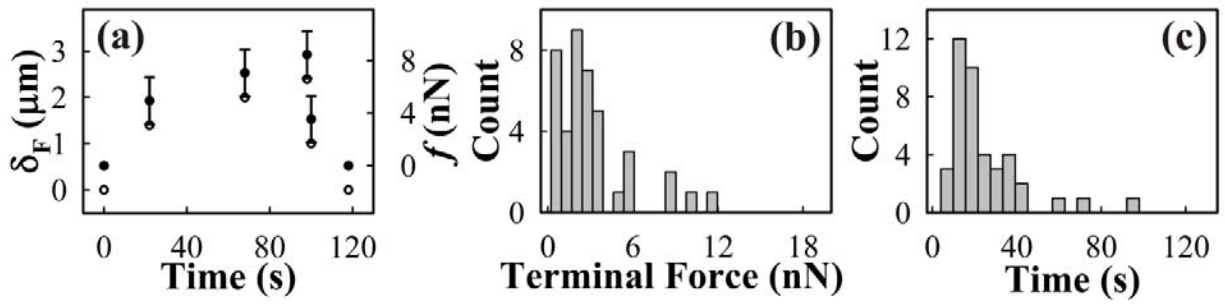

Figure 6. (a) Apical pseudopod induced deflection (unfilled circles) and force (filled circles) measured during the event depicted in figure 5. The error bars reflect the propagated uncertainties of δ_F and k_{res}. (b) Distribution of the terminal forces obtained from 41 pseudopod-fiber deflection events. (c) Distribution of contact durations obtained from the same set of 41 events.

Figure 6(a) shows the fiber-end deflection-values $\delta_F(L)$ (unfilled circles) corresponding to the apical pseudopod deflection event of figure 5(a)-(f). This fiber—wire 25 in Table 1—was found to have a spring constant k_{res} of 3.5 ± 0.3 nN/μm. Conversion of the δ_F-values to forces f via Hooke's law ($f = \delta_F k_{res}$) yields the filled circles in figure 6(a). These data show that f reaches 8.5 nN without breaking contact. A total of 41 apical pseudopod-fiber deflection events were observed in this study. Figure 6(b) depicts the distribution of the terminal forces for these events. *Terminal force* refers to the force applied to the fiber the instant before it recoiled to its neutral position. The average terminal force was 3.1 ± 2.7 nN. Figure 6(c) depicts the distribution of the durations of these events. The average contact duration was 23.4 ± 18.5 s.

4. Discussion

This study presents methodology for fabricating cantilevered cellular force sensors composed of PEDOT fibers grown from maneuverable substrates. The diameter and length of a fiber are user-controlled during the growth process and, consequently, the spring constants of the fibers may be controlled across reasonably narrow ranges as shown in the inset to figure 4(a). These force sensors are calibrated either by

measuring the fibers' spring constants directly via AFM or, more conveniently, by finding their resonance frequencies for transverse vibration. The near-unity slope of figure 4(a) implies that the resonance frequency calibration method [*i.e.* equation (2)], though approximate, is sufficiently accurate to forgo the more laborious AFM method. In applying (2) to the PEDOT fibers, we assume that the fiber bends like a hypothetical uniform fiber having a particular radius and vibrates like a uniform fiber of the same radius. However, the PEDOT fibers are radially non-uniform [inset of figure 1(c)]. For structurally non-uniform cantilevers, this assumption is not strictly true. The spring constant and the resonance frequencies of a cantilever are derived from different forms of Newton's 2nd Law: for the former, there is no net torque on the fiber; for the latter the net torque varies periodically with time. Hence, it is somewhat fortuitous that the resonance-based spring constant determinations were found to be accurate [figure 4(a)]. The theoretical analysis required to quantify the limits of this approximation lies beyond the scope of this work. However, because the resonance-method is in wide use in the calibration of micro- and nano-cantilevers, we feel that elucidation of the limits of this assumption is needed, and will present such an analysis in a forthcoming work.

Because the fibers are radially non-uniform and somewhat axially asymmetric, concern over the anisotropy of their spring constants arises. Figure 4(b) shows that the resonance frequency values in planes-of-bending that differ by 90^o of axial rotation are essentially equal for a given fiber. Because ω_0 predicts k_F to a reasonable degree of accuracy (discussed above), this finding implies that the spring constants in orthogonal bending planes are essentially the same; thus, we do not observe a significant degree of bending anisotropy. A related concern is that the fibers grow unevenly, causing their foremost tips to have different average radii than their bases. A radially uniform fiber has a resonance frequency of $\omega_0 = 1.75\sqrt{E\rho^{-1}}rL^{-2}$. Hence, the inset to figure 4(b) shows that the PEDOT fibers resonate like radially uniform fibers as shortening the fibers does not change the slope ($1.75\sqrt{E\rho^{-1}}r$) of their ω_0 versus L^{-2} plots. These data also provide further confirmation that fibers grown under the same controlled conditions have

similar structures, as each of the four data-sets shown in this plot has the same slope. Hence, these findings presented in figures 4(a) and (b) establish a basis for calibrating these fibers via the comparatively straight-forward resonance method.

Typical lengths of the PEDOT fibers are ~20 μm, which provides sufficient reach to cleanly interface the tip of a fiber with a subcellular target on a cell without forming unintentional secondary contacts to the cell. To demonstrate this capability, we have resolved the dynamical forces that arise at individual adhesive contacts between the tips of apical pseudopods and the PEDOT cantilevers. Most prior work on pseudopod dynamics has regarded motility on planar substrates such as Petri dishes and microscope slides. However, apical pseudopod dynamics are required of *D. discoideum* in nature where the local topography of forest floors—crevices and debris—necessitates off-plane motion of a cell as it transfers from one surface to another. By employing the dynamical force sensors, the present study found the average terminal force exerted during the apical pseudopod-secondary substrate adhesive contacts to be 3.1 ± 2.7 nN and the average duration of these contacts to be 23.4 ± 18.5 s. This period compares well to the 19.4 ± 8.2 s lifetimes of the adhesive contacts made by actin foci to *basal* substrates [41], suggesting that the adhesive structures at the apical pseudopod-tips may be actin foci. However, no external forces were applied to the actin-foci in this prior study (although internal forces could have been present) [41]. This detail is significant because the application of a force against a bond accelerates the dissociation rate of the bond [42]. Hence, when a pulling force is applied against an actin focus, it is expected to decay more rapidly than the 19.4 s average lifetime in the unforced case. On the other hand, apical contacts can survive for 23.4 s under few nano-Newton external forces [figures 6(a) and (b)]. This comparative robustness is expected to increase the probability that apical contacts survive while the pre-existing basal contacts (actin foci) decay, as required for inter-substrate (basal-to-apical) transfer. Further investigation into this mechanism will be undertaken in a future study.

5. Conclusion

This study has presented an innovative methodology for the electrochemical fabrication of cellular force sensors composed of cantilevered PEDOT fibers. Calibration of the force sensors is straight-forward via measurement of the transverse resonance frequencies of the fibers. By employing these fibers to characterize the dynamics of apical pseudopod-substrate adhesive contacts of *D. discoideum* cells, we have shown that these cantilevers are effective, high aspect ratio cellular force probes that may be positioned independently around the cell and can interface with sub-micron targets without forming unintentional secondary contacts to the cell. These capabilities will permit further statistical characterization of the durations and magnitudes of the forces exerted at individual apical and lateral pseudopod substrate contacts, as a means of elucidating the physical basis of pseudopod-substrate adhesion. We also note that the dimensions and maneuverability of the PEDOT force probes will likely permit characterization of the dynamics at other interesting adhesive entities such as the setae and spatulae of gecko feet [43] and the micro-bristles of beetle tarsi [44], which have dimensions comparable to *D. discoideum* pseudopods.

Acknowledgement. This work was partially supported by National Science Foundation grants PHY-0646966 (BNF) and DMR-0603144 (BML). We thank Professor Robert Szoszkiewicz for helpful suggestions regarding cantilever calibration.

References

[1] Friedl P, Borgmann S and Broecker E B 2001 Amoeboid leukocyte crawling throgh extracellular matrix: lessons from the *Dictyostelium* paradigm of cell movement *J. Leukoc. Biol.* **70** 491-509

[2] Muller A, Homey B, Soto H, Ge N F, Catron D, Buchanan M E, McClanahan T, Murphy E, Yuan W, Wagner S N, Barrera J L, Mohar A, Verastegui E and Zlotnik A 2001 Involvement of chemokine receptors in breast cancer metastasis *Nature* **410** 50-6

[3] Stossel T P 1994 The machinery of blood cell movements *Blood* **84** 367-79

[4] Yumura S and Kitanishi-Yumura T 1990 Fluorescence-mediated visualisation of actin and myosin filaments in the contractile membrane-cytoskeleton complex of *Dictyostelium discoideum Cell Struct. Funct.* **15** 355-64

[5] Ren X S, Kiosses W B, Sieg D J, Otey C A, Schlaepfer D D and Schwartz M A 2000 Focal adhesion kinase suppresses Rho activity to promote focal adhesion turnover *J. Cell .Sci.* **113** 3673-8
[6] Galbraith C G and Sheetz M P 1997 A micromachined device provides a new bend on fibroblast traction forces *Proc. Natl. Acad. Sci.* **94** 9114-8
[7] Walter N, Selhuber C, Kessler H and Spatz J P 2006 Cellular unbinding forces of initial adhesion processes on nanopatterned surfaces probed with magnetic tweezers *Nano Lett.* **6** 398-402
[8] Vogel V and Sheetz M 2006 Local force and geometry sensing regulate cell functions *Nature Reviews: Molecular Cell Biology* **7** 265-75
[9] Devreotes P N and Zigmond S H 1988 Chemotaxis in eukaryotic cells: a focus on leukocytes and *Dictyostelium Annual Review of Cell Biology* **4** 649-86
[10] Bailly M, Condeelis J S and Segall J E 1998 Chemoattractant-induced lamellipod extension *Microsc. Res. Technol.* **43** 433-43
[11] Stossel T P, Hartwig J H, Janmey P A and Kwiatkowski D J 1999 Cell crawling two decades after Abercrombie *Biochem. Soc. Symp.* **65** 267-80
[12] Friedl P, Entschladen F, Conrad C, Niggermann B and Zanker K S 1998 CD4+ T lymphocytes migrating in three dimensional collagen lattices lack focal adhesions and utilize beta1 integrin-independent strategies for polarization, interaction with collagen fibers and locomotion *Eur. J. Immunol.* **28** 2331-43
[13] Friedl P and Weigelin B 2008 Interstitial leukocyte migration and immune function *Nature Immunology* **9** 960-9
[14] Harris A K, Stopak D and Wild P 1980 Silicone substrata: a new wrinkle in the study of cell locomotion *Science* **208** 177-9
[15] Schwartz U S, Balaban N Q, Riveline D, Bershadsky A, Geiger B and Safran S A 2002 Calculation of forces at focal adhesions from elastic substrate data: the effect of localized force and the need for regularization *Biophys. J.* **83** 1380-94
[16] Pfister G, Stroh C M, Perschinka H, Kind M, Knoflach M, Hinterdorfer P and Wick G 2005 Detection of HSP60 on the membrane surface of stressed human endothelial cells by atomic force and confocal microscopy *Journal of Cell Science* **118** 1587-94
[17] Helenius J, Heisenberg C-P, Gaub H E and Muller D J 2008 Single-cell force spectroscopy *Journal of Cell Science* **121** 1785-91
[18] Sun Z, Martinez-Lemus L A, Trache A, Trzeciakowski J P, Davis G E, Pohl U and Meininger G A 2005 Mechanical properties of the interaction betwen fibronectin and alpha5beta1-integrin on vascular smooth muscle cells studied using atomic force microscopy *Am. J. Physiol.* **289** H5226-H2535
[19] Trache A, Trzeciakowski J P, Gardiner L, Sun Z, Muthuchamy M, Guo M, Yuan S Y and Meininger G A 2005 Histamine effects on endothelial cell fibronectin interaction studied by atomic force microscopy *Biophys. J.* **89** 2888-98
[20] Friedrichs J, Helenius J and Mueller D J 2010 Stimulated single-cell force spectroscopy to quantify cell adhesion receptor crosstalk *Proteomics* **10** 1455-62
[21] Hoffmann S, Hosseini B H, Hecker M, Louban I, Bulbuc N, Garbi N, Wabnitz G H, Samstag Y, Spatz J P and Haemmerling G J 2011 Single cell force spectroscopy of T cells recognizing a myelin-derived peptide on antigen presenting cells *Immunology Letters* **136** 13-20
[22] Hoffmann S C, Wabnitz G H, Samstag Y, Moldenhauer G and Ludwig T 2011 Functional analysis of bispecific antibody (EpCAMxCD3)-mediated T-lymphocyte and cancer cell interaction by single-cell force spectroscopy *International Journal of Cancer* **128** 2096-104
[23] Evans E, Ritchie K and Merkel R 1995 Sensitive force technique to probe molucular adhesion and structural linkages at biological interfaces *Biophys. J.* **68** 2580-7
[24] Litvinov R I, Shuman H, Bennett J S and Weisel J W 2002 Binding strength and activation state of single fibrinogen-integrin pairs on living cells *Biophys. J.* **84** 1252-62

[25] Paneru G, Thapa P S, McBride S P, Nichols D M, Law B M and Flanders B N 2011 Forces at individual pseudopod-filament adhesive contacts *Appl. Phys. Lett.* **99** 093702
[26] Qiao Y, Chen J, Guo X, Cantrell D, Ruoff R and Troy J 2005 Fabrication of nanoelectrodes for neurophysiology: cathodic electrophoretic paint insulation and focused ion beam milling *Nanotechnology* **16** 1598-602
[27] Thapa P S, Barisci J N, Yu D J, Wicksted J P, Baughman R and Flanders B N 2009 Directional growth of conducting polypyrrole and polythiophene nanowires *Appl. Phys. Lett.* **94** 033104
[28] Thapa P S, Ackerson B J, Grischkowsky D R and Flanders B N 2009 Directional growth of metallic and polymeric nanowires *Nanotechnology* **20** 235307
[29] Flanders B N 2012 Directed Electrochemical Nanowire Assembly: Precise Nanostructure Assembly via Dendritic Solidification *Mod. Phys. Lett. B* **26** 1130001
[30] Ozturk B, Talukdar I and Flanders B N 2007 Directed growth of diameter-tunable nanowires *Nanotechnology* **18** 365302
[31] Yang S and Saif T 2005 Micromachined force sensors for the study of cell mechanics *Rev. Sci. Instrum.* **76** 044301
[32] Gates R S and Reitsma M G 2007 Precise atomic force microscope cantilever spring constant calibration using a reference cantilever array *Rev. Sci. Instrum.* **78** 086101
[33] Gao R, Wang Z L, Bai Z, deHeer W A, Dai L and Gao M 2000 Nanomechanics of individual carbon nanotubes from pyrolytically grown arrays *Phys. Rev. Lett.* **85** 622-5
[34] Zhou J, Lao C S, Gao P, Mai W, Hughes W L, Deng S Z, Xu N S and Wang Z L 2006 Nanowire as pico-gram balance at workplace atmosphere *Sol. State. Comm.* **139** 222-6
[35] Landau L D and Lifshitz E M 2000 *Theory of Elasticity* (Oxford: Butterworth-Heinemann)
[36] Watts D J and Ashworth J M 1970 Growth of myxameobae of the cellular slime mould Dictyostelium discoideum in axenic culture *The Biochemical Journal*. **119** 171-4
[37] Chaudhuri O, Parekh S, Lam W and Fletcher D 2009 Combined atomic force microscopy and side-view optical imaging for mechanical studies of cells *Nature Methods* **6** 383-7
[38] Okuzaki H and Ishihara M 2003 Spinning and characterization of conducting microfibers *Macromol. Rapid Commun.* **24** 261-4
[39] Tahk D, Lee H H and Khang D Y 2009 Elastic moduli of organic electronic materials by the buckling method *Macromolecules* **42** 7079-83
[40] Nu L, Kvarnström C, Fröberg K and Ivaska A 2001 Electrochemically controlled surface morphology and crystallinity in poly (3.4-ethylenedioxythiophene) films *Synthetic Metals* **122** 425-9
[41] Uchida K S K and Yumura S 2004 Dynamics of novel feet of *D. discoideum* during migration *J. Cell .Sci.* **117** 1443-55
[42] Hänggi P, Talkner P and Borkovec M 1990 Reaction rate theory: 50 years after Kramers *Rev. Mod. Phys.* **62** 251-342
[43] Huber G, Mantz H, Spolenak R, Mecke K, Jacobs K, Gorb S N and Arzt E 2005 Evidence for capillarity contributions to gecko adhesion from single spatula nanomechanical measurements *Proc. Natl. Acad. Sci.* **102** 16293-6
[44] Eisner T and Aneshansley D J 2000 Defense by foot adhesion in a beetle (Hemisphaerota cyanea) *Proc. Natl. Acad. Sci.* **97** 6568-73